Single-Source Pulsed Laser Deposition of $MAPbI_3$

Tatiana Soto-Montero[1], Wiria Soltanpoor[1], Suzana Kralj[1], Yorick A. Birkhölzer[1], Zdenek Remes[2], Martin Ledinsky[2], Guus Rijnders[1], Monica Morales-Masis[1]

[1] MESA+ Institute for Nanotechnology, University of Twente, Enschede 7500 AE, The Netherlands

[2] Institute of Physics, Academy of Science of the Czech Republic, Cukrovarnická 10, Prague 162 00, Czech Republic

***Abstract*—As the employment of halide perovskite films in single-junction and tandem solar cells continues to soar, there is a strong drive -from academia to industry- to produce these films using dry processes, avoiding the use of toxic solvents. Vapor deposition methods such as co-evaporation have shown advantages of solvent-free approaches to produce high-efficiency solar cells. However, co-evaporation requires the use of multiple sources that challenge the deposition rate control of complex halide perovskite compositions. Here, Pulsed Laser Deposition (PLD) is proposed as an alternative method to deposit hybrid halide perovskites films from a single-source and following a fully dry approach. We use the archetypical methylammonium lead iodide ($MAPbI_3$) to demonstrate the formation of high-quality films with optimal optoelectronic properties by PLD on various substrates for single-junction and tandem devices. Furthermore, the important role of the PLD target composition and deposition parameters to achieve control over film microstructure and optoelectronic properties is discussed. The controlled conformal growth provided by PLD demonstrated in this work with $MAPbI_3$ on device-relevant substrates will broaden opportunities to explore PLD of more complex hybrid halide perovskite compositions for efficient, stable, and scalable solar cell devices.**

Keywords—halide perovskites, methylammonium lead iodide, pulsed laser deposition, conformal growth, thin-films, single-source, dry methods, physical vapor deposition.

I. Introduction

Hybrid halide perovskites have enticed the photovoltaic community's interest since 2012 when solar cell devices with power conversion efficiencies (PCE) exceeding 9% were demonstrated [1]. These materials have an ABX_3 stoichiometry, where A^+ is a monovalent organic cation such as methylammonium ($CH_3NH_3^+$), B^{+2} is a divalent inorganic cation such as lead (Pb^{+2}), and X^- is a halide such as iodide (I^-) or bromide (Br^-). The most studied halide perovskite composition is methylammonium lead iodide $CH_3NH_3PbI_3$ ($MAPbI_3$). Its attractive optoelectronic properties fulfill most of the requirements to harvest solar energy, such as high absorption coefficient (in the order of 10^5 cm^{-1} over the whole visible spectrum), long charge carrier diffusion lengths ($\geq$ 1 µm), ambipolar charge transport, low exciton blinding energy ($\leq$ 16 meV), tunable bandgap, and defect tolerance [2]. The latter means that halide perovskites can be utilized in thin-film form for solar cells without the need for expensive and time-consuming methods to achieve high-quality films. A variety of synthetic methods have been demonstrated to grow halide perovskite thin films, such as solution-based, hybrid, and vacuum-based methods [3]. Optimized solution-based methods, particularly the spin coating method, have proven a PCE up to 25.5 % in small area devices [4]. However, the application of the spin coating method becomes challenging for the integration into heterostructures such as monolithic tandem devices and large area depositions [5]. Therefore, exploring novel fabrication methods with the possibility of upscaling and incorporating heterostructures for large area depositions of single-junction and tandem devices are therefore required [3], [6]–[8].

Pulsed laser deposition (PLD) is a physical vapor deposition technique (PVD) widely used to grow oxide perovskites, as this technique allows near-stoichiometric transfer of the complex (multi-compound) oxide target materials to thin films [9]. The conformal growth of films without damaging the underlayers and scalability of PLD have also been demonstrated recently for contact materials, making this technique highly attractive for full solar cell devices [10]. In PLD, a high energy laser pulse ablates a target comprised of the material of interest. During this process, the photons interact with the material in the target, exciting the bonded electrons and transferring their energy to the lattice via the electron-phonon coupling [11]. This results in the dissociation of the target constituents forming a confined plasma plume that expands towards the substrate. With every pulse, material is deposited on a substrate and by nucleation and growth processes, a thin film is formed [12].

One of the most compelling advantages of PLD is the deposition of thin films with complex (multicompound) compositions from a single solid target [12]. For instance, the deposition of $MAPbI_3$ by other PVD methods such as co-evaporation will require the use of two sources [13]. Other reported multi-cation compositions, $FA_{0.7}Cs_{0.3}Pb(I_{0.9}Br_{0.1})_3$ [14] and $Cs_{0.5}FA_{0.4}MA_{0.1}Pb(I_{0.83}Br_{0.17})_3$ [15], require three and four sublimation sources, respectively, which also increase the challenge of stoichiometry control. Not only, a single PLD target can have the precursor stoichiometry of preference, but also the versatility of PLD allows tuning the film properties by varying the different deposition parameters, among others, deposition pressure, laser spot size, and substrate type.

Recent reports have demonstrated PLD of $CsSnI_3$ [16], $Cs_2AgBiBr_6$ [17], $MAPbI_{3-x}A_x$ (A= Cl or F) [18], $MASnI_3$ [18], $CsPbBr_3$ [19], $MAPbBr_3$ [20], and $(FA)_{1-x}(MA)_xSnI_3$ [21]. Here we demonstrate the controlled growth of $MAPbI_3$ by PLD on

various substrates, including relevant substrates for single-junction and tandem devices. Below we describe the critical PLD parameters and the role of target composition to achieve $MAPbI_3$ films with optimum structural and optical properties.

II. Experimental Details

Solid targets with different ratios of PbI_2 (Alfa Aesar 99.99 %) and MAI (Greatcell solar 99.99 %) were fabricated by mechanochemical synthesis (MCS), a process that will be described in the next section.

$MAPbI_3$ thin films were deposited onto Si substrates (with native SiO_2) for structural characterization, fused silica for optical characterization, ITO/SnO_2/PCBM as a device relevant stack, and textured silicon wafers for conformal layer growth demonstration. PLD was performed in a vacuum chamber, base pressure of $\leq 4.0 \times 10^{-6}$ mbar, variable working pressures controlled via the introduction of Ar gas, substrate at room temperature, laser frequency of 4 Hz, target to substrate distance of 60 mm, and at a fluence of 0.3 J cm^{-2}. Different target compositions were tested, but the optimization process was performed on the target with a 1:8 (PbI_2: MAI) ratio while varying the laser spot size from 1mm^2 to 2.5mm^2. The ablation of the solid target was done with a KrF (λ = 248 nm) excimer laser (Coherent, Complex-Pro).

The microstructure and phase of the solid targets and films were characterized via X-ray diffraction (XRD) using a PANalytical X'Pert Pro Materials Research Diffractometer.

Optical absorption coefficient measurements were performed using photothermal deflection spectroscopy (PDS) in a broad spectral range from ultraviolet to infrared region 400−1200 nm. Optical absorbance spectra were measured by a Perkin Elmer UV/vis/NIR spectrometer Lambda 950 with an integrating sphere. Atomic force microscopy (AFM) on tapping mode and high-resolution scanning electron microscopy (HR-SEM) were employed to study the film morphologies.

III. Results and Discussion

A. Solid Target Fabrication and Characterization

In contrast to the conventional solution-based processes where the halide salt precursors are dissolved in common organic solvents such as dimethylformamide (DMF) and/or dimethyl sulfoxide (DMSO), PLD requires a solid target containing the material of interest, which can be processed via wet-chemistry [22] or via dry mechanochemical synthesis (MCS) [23]. During mechanochemistry, the perovskite precursors experience a solid-state chemical reaction prompted by the absorption of mechanical energy [24]. MCS allows solvent-free processing and a refined control over the stoichiometry of the final perovskite powder mixture. The demand for the synthesis of inorganic and hybrid halide perovskites by MCS has increased in just a few years due to the superior stability of the high-purity materials. Also, compared to wet chemistry, MCS is not limited by the incompatible solubility of the halide salt precursors [22], [23].

MCS of halide perovskites can be achieved by a simple process such as reactive grinding using a mortar and pestle [25] or by high-energy reactive grinding and milling using a planetary ball-mill system [26]. During this study, we use a homemade rotary ball-mill (RBM) process in which reactive grinding and milling are the main processes to promote the chemical reaction of the starting materials. Stoichiometric and off-stoichiometric amounts of lead iodide (PbI_2) and the organic methylammonium iodide (CH_3NH_3I or MAI) salts were introduced in an N_2-filled vessel containing zirconia balls and subsequently ball-milled for four days. During this period, the gravitational force creates a continuous impact between the zirconia balls and the powder promoting the milling process, but at the same time, the impact of the powder precursors between zirconia balls causes the shear and thus the powder grinding process [26]. The mixing of stoichiometric precursors showed an incubation time of about six hours, which is required to obtain the first $MAPbI_3$ diffraction peaks corresponding to the tetragonal phase as observed by XRD. Once the reaction is done, the perovskite powder is loaded into a pressing die to turn the powder into compact, solid targets.

Dense targets are desired to promote the ablation of the material without ejecting big particles that can compromise the final film morphology. However, one of the challenges of the deposition of hybrid halide perovskites films from a single source is the control of the scattering of lighter elements, as represented in Fig. 1 [20], [21]. Thus, multiple targets with various organic to inorganic salts ratios were prepared to investigate the effect of highly dissimilar atomic masses of the target constituents (H, C, N, I, Pb) on the transfer efficiency upon laser ablation (KrF, 248 nm).

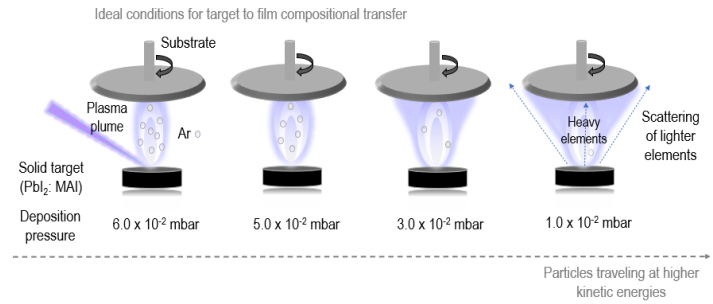

Fig. 1. Illustration representing the plume shape during PLD at different deposition pressures (while keeping constant other PLD parameters: target composition, fluence, spot size, and frequency). At high pressures, the thermalization of particles allows the nearly equal transfer (smaller plasma plume size). In contrast, the scattering of light elements is more likely to occur at low pressures (less organic species arriving at the substrate).

Fig. 2 displays the XRD patterns of the targets with a 1:1, 1:4, 1:6 and 1:8 molar ratio of PbI_2:MAI. All targets are identified as mixtures of the black tetragonal $MAPbI_3$ phase and unreacted PbI_2 and MAI. The increase of MAI peaks intensity follows the organic enrichment of the target.

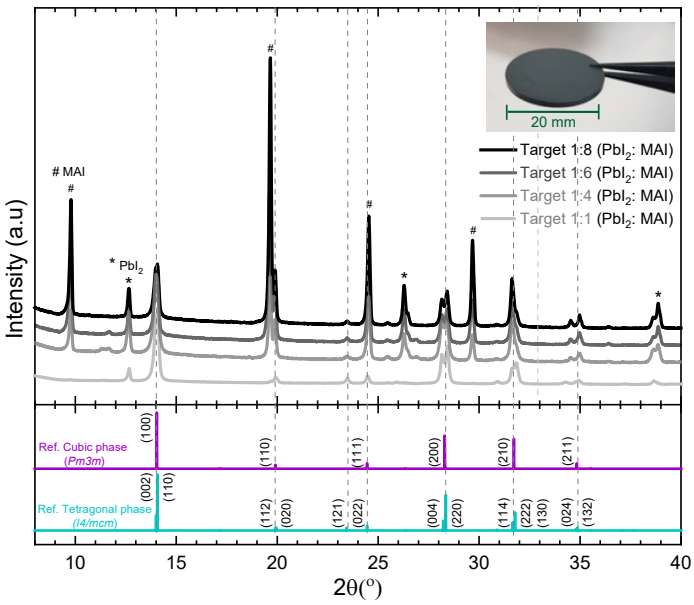

Fig. 2. X-ray diffraction (XRD) patterns of the solid targets with 1:1, 1:4, 1:6 and 1:8 (PbI_2:MAI) ratios. For comparison, the cubic *Pm3m* and tetragonal *I4/mcm* phase reference spectrums are plotted below. Inset: $MAPbI_3$ target 1:1.

B. Pulsed Laser Deposition of $MAPbI_3$ Films

To control the deposition pressure during PLD, an inert gas (Ar) is introduced in the chamber. The main function of this gas is to reduce the kinetic energy of the particles in the plasma plume, acting as a moderator of the arriving species, as well as promoting thermalization of the ablated species. Choosing an optimum range of deposition pressures is therefore of utmost importance to achieve the desired composition, controlling the scattering of lighter elements and keep the films integrity while avoiding undesirable (preferential) re-sputtering of the thin film surface. In addition to the deposition pressure, the composition of the target also plays an important role in the final composition of the films. To study these effects, solid targets with PbI_2:MAI ratios of 1:1, 1:6, 1:8 were used to deposit thin films.

The first approach was performed employing the target 1:1 (PbI_2:MAI) in a range of deposition pressures between ~ 10^{-1} - 10^{-3} mbar. Fig. 3.a. displays the XRD patterns of the deposited 200 nm-thick films. All films deposited from the 1:1 (PbI_2:MAI) target resulted in PbI_2-rich films as determined by XRD. We explain the MAI losses resulting from the scattering of organic species during deposition at relatively low deposition pressures (~10^{-3} mbar). When increasing the deposition pressure (~10^{-1} mbar), the films are still PbI_2 rich but with some low-intensity peaks that may indicate the beginning of the $MAPbI_3$ phase formation. This high pressure (~10^{-1} mbar), however, resulted in the formation of porous films. Therefore, a pressure in the range of ~10^{-2} mbar, was chosen for the PLD optimization with MAI-rich targets.

Films deposited from targets with 1:6 and 1:8 (PbI_2:MAI) ratios and a pressure of 6.0 x 10^{-2} mbar, resulted in tetragonal $MAPbI_3$ phase formation as confirmed by the XRD patterns presented in Fig. 3.a. As described in Fig. 1, we speculate preferential scattering of the light elements at pressures lower than 1 x 10^{-2} mbar, causing non-uniform or non-stoichiometric films. One way to alleviate this is by increasing the deposition pressure to a range between 6.0 x 10^{-2}-3.0 x 10^{-2} mbar and using off-stoichiometric targets as demonstrated in this work.

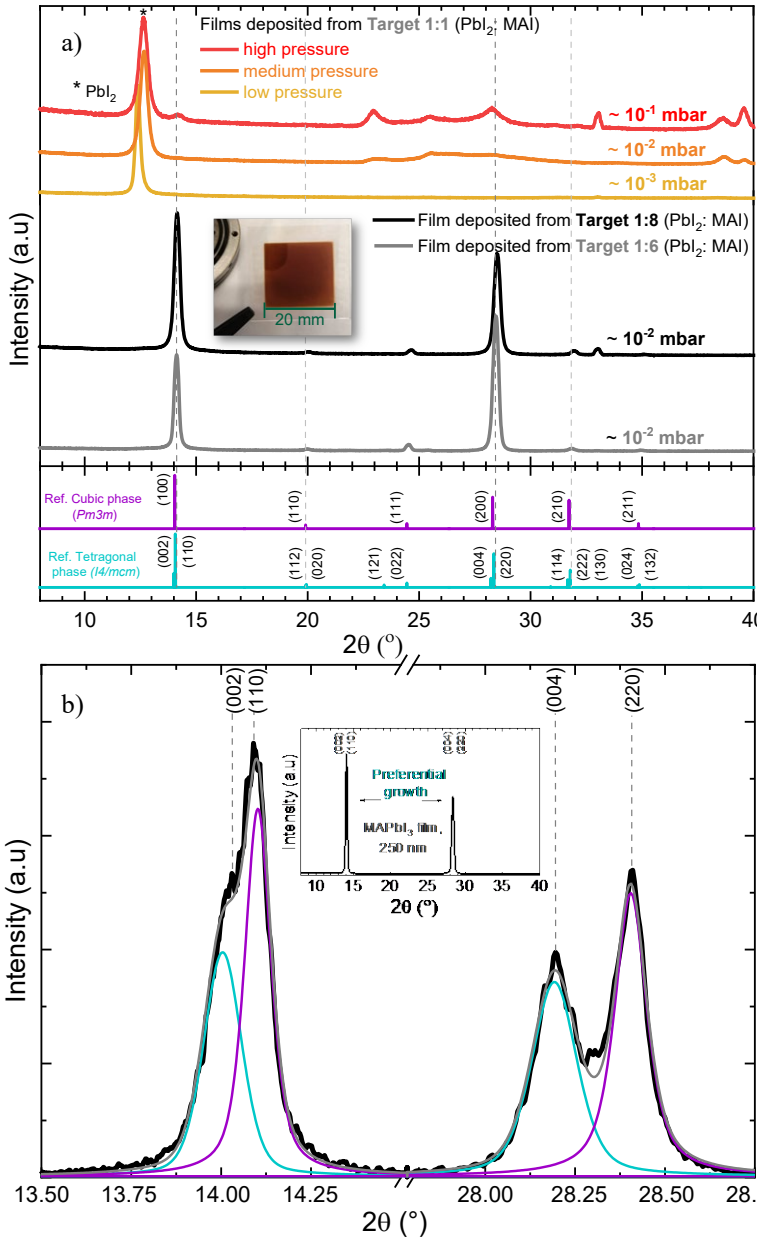

Fig. 3. Structural properties of the optimized PLD-grown $MAPbI_3$ films. a) X-ray diffraction (XRD) patterns of the films from targets 1:1, 1:6 and 1:8 PbI_2:MAI ratios. b) Monochromatic triple-axis configuration measurements confirming the tetragonal photoactive black phase formation (inset: wide-angle XRD pattern of the highly-oriented film deposited on Si).

Not only the excess of MAI in the target allowed for the formation of $MAPbI_3$ film, but also the laser fluence strongly affects the stoichiometry, microstructure, deposition rate, and film thickness. We found an optimum fluence range of 0.25-0.45 J/cm^2 to achieve control over the film density and microstructure without compromising the film composition. All depositions are performed at room temperature, and no post-treatment is

employed, indicating an advantage for deposition on temperature-sensitive substrates. Furthermore, to distinguish the cubic and tetragonal polymorphs of $MAPbI_3$, high resolution, monochromatic XRD measurements were performed in triple-axis configuration. These experiments revealed the characteristic peak splitting at ~14° and ~28° (2Θ), corresponding uniquely to the tetragonal photoactive black phase of $MAPbI_3$ (Fig. 3.b).

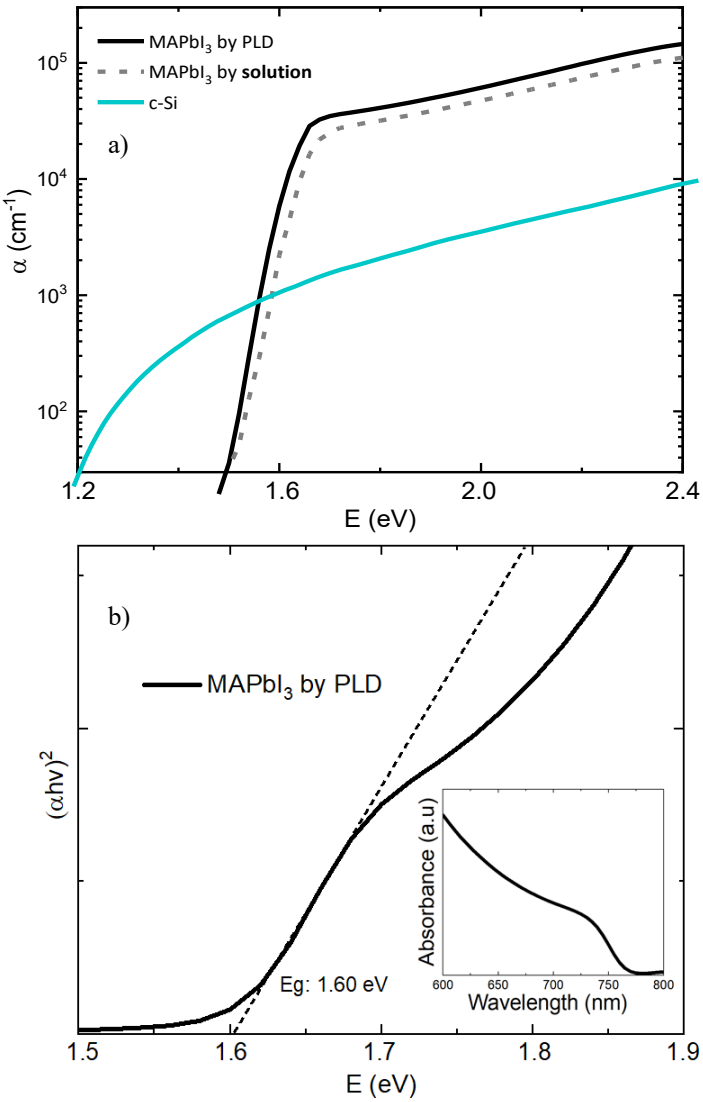

Fig. 4. Optical properties of the optimized PLD-grown $MAPbI_3$ films. a) Absorption coefficient plot of 200 nm-thick $MAPbI_3$ films prepared by PLD (solid line) and for comparison spin-coated $MAPbI_3$ films (dash line) and c-Si (blue line). b) Tauc plot and estimated bandgap (inset: absorbance plot).

The optical properties of optimized tetragonal $MAPbI_3$ films are presented in Fig. 4. The absorption coefficient confirms high light absorption across the whole visible spectrum and a sharp absorption edge, well comparable with reference solution-based $MAPbI_3$. This proves the optical quality and indicates the potential to obtain high open-circuit voltages on solar cells based on these materials [27]. Additionally, undetectable absorption in the infra-red part of the spectra makes this material interesting for tandem devices. The Tauc plot for direct transition indicates a bandgap of 1.60 eV, consistently with the reported values for $MAPbI_3$ [27].One of the more significant findings to emerge from this study is that high-quality $MAPbI_3$ films can be grown employing an alternative vapor deposition method (PLD) from a single source. Furthermore, the target stoichiometry and the deposition pressure plays a key role to control the film composition, microstructure, and optical properties. Our optimized films were grown at 6.0 x 10^{-2} mbar from a target containing a 1:8 (PbI_2:MAI) ratio. For the rest of the optimizations, we kept working with the 1:8 (PbI_2:MAI) target because it gave us a broader window to tune key deposition parameters to optimize films on other relevant substrates.

C. Effect of Substrate on PLD $MAPbI_3$ Film Growth Orientation

It has been reported that the substrate has a strong effect on the final film morphology of thermally evaporated $MAPbI_3$ and other halide perovskites [28], [29]. To test if this is also the case for PLD grown films, and after confirming high-quality films on silicon and glass substrates (Fig. 3,4), we proceeded with the PLD growth of $MAPbI_3$ on contact layers. The chosen substrate stack is that of a NIP structure: Glass/ITO/SnO_2/PCBM. Tin(IV) oxide (SnO_2) is one of the preferred electron transport layers (ETL) because of its suitable energy band alignment with $MAPbI_3$, high optical transmission, and low-temperature processability [30].

Fig. 5. XRD patterns of films grown on Si/SiO_x substrates and on

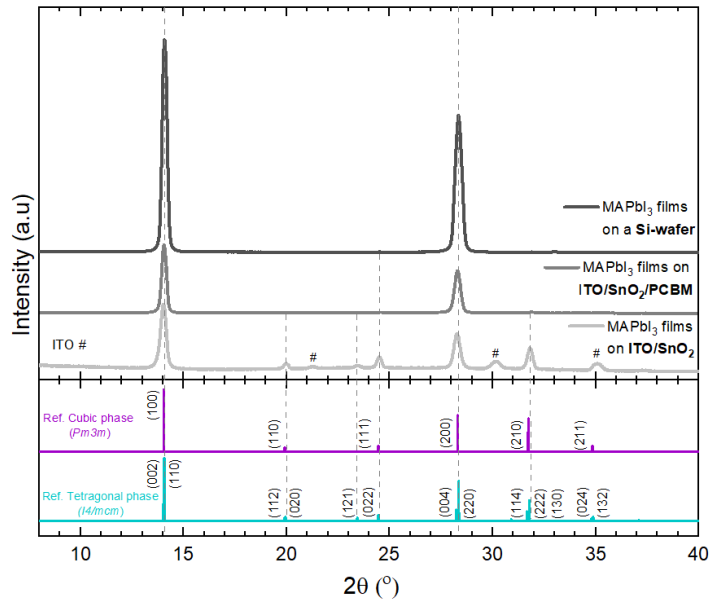

ITO/SnO_2 and ITO/SnO_2/PCBM contact layers, resulting in thin films presenting the photoactive tetragonal phase. The dashed lines indicate the different growth orientations.

Fig. 5 reveals the XRD patterns of films grown on Si substrates, ITO/SnO_2, and ITO/SnO_2/PCBM contact layers. The films grown on Si present high crystallinity and a highly-oriented film growth (002)/(110), whereas films grown on ITO/SnO_2/PCBM displayed an extra orientation (022) at 24.45, 2θ. On the contrary, the films grown on ITO/SnO_2 lost the preferential orientation and the high crystallinity (some ITO peaks are also visible). Cojocaru *et al*. also found different

crystal growth orientations when growing $MAPbI_3$ film by co-evaporation on ITO/TiO_2 vs ITO/TiO_2/PCBM. The films growth on PCBM showed a slightly better crystallinity and a preferential (110) orientation as compared to films grown directly on TiO_2 [28]. The employment of PCBM not only changes the surface energy of the substrate but also modifies the preferential growth of films. These findings, together with the reported high-quality films, reported better carrier-selective interface with the absorber, led us to keep working with the ITO/SnO_2/PCBM stack [28], [29], [31].

D. Approaches to improve film's morphology and surface roughness

Another important characteristic of high-quality films is surface roughness. The final film morphology is influenced not only by the deposition parameters but also by the quality of the target and its ablation. By ensuring a uniform and dense 1:8 (PbI_2:MAI) ratio target and controlling the ablation spot size, we observe an improvement of the surface morphology. Fig. 6 show the improvement of surface morphology as revealed AFM images when changing the laser spot size from 1.0 to 2.5 mm^2 while keeping a constant fluence of 0.3 J/cm^3. This means that the instantaneous growth speed (per pulse) is much larger for 2.5 mm^2 and with that the growth processes are affected. Fig. 6 presents the film surface morphology evolution, from large unwanted surface microparticles (left) to a uniform film with RMS roughness of 12.4 nm (right). Importantly, the crystallinity and optical properties were invariant, but an extra advantage was noticed on the deposition rate. When using 2.5 mm^2 spot size, it is possible to grow 500 nm thick films of $MAPbI_3$ in 36 min, approximately four times faster than other well-known PVD techniques [28].

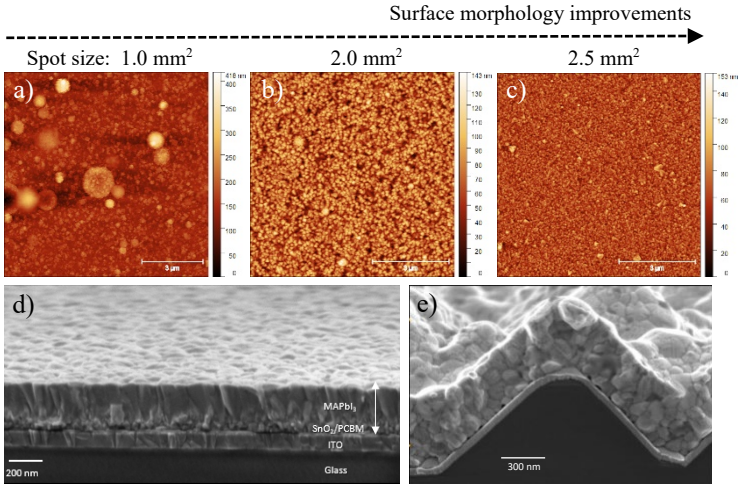

Fig. 6. Films morphology optimization and conformal growth demonstration. Atomic Force Microscopy (AFM) images on tapping mode (8x8 µm scans) of films deposited using different laser spot sizes: a) 1.0 mm^2 (rms: 33.9 nm), b) 2.0 mm^2 (rms: 18.7 nm), and c) 2.5 mm^2 (rms: 12.4 nm). d) Cross-sectional SEM images of films deposited on Glass/ITO/SnO_2/PCBM. e) Conformal growth of $MAPbI_3$ on textured silicon wafers typically used for silicon bottom cells.

Films morphology Fig. 6 shows the cross-section electron micrographs of films grown on glass/ITO/SnO_2/PCBM substrates (Fig. 6d) and textured Silicon wafers (Fig. 6e). We demonstrate film thicknesses from 350-500 nm using different numbers of pulses during the deposition. This provides for thickness tuning based on particular device requirements (single- or multi-junction) [32]. Fig. 6e demonstrates the potential of PLD for conformal growth of $MAPbI_3$ films using a single-source dry process. This opens the possibility for further application of PLD for other halide perovskite families, including wide-bandgap perovskites useful for monolithic tandem devices.

IV. Summary of the Work

We presented the growth of high-quality $MAPbI_3$ thin films by PLD as a promising vapor deposition technique employing a single-source for room temperature depositions on several substrates. Understanding the influence of the different deposition parameters on the final film properties is essential to build synthesis-structure-properties relations to improve the film quality and ultimately the final device performance. The versatility of PLD to grow hybrid halide perovskites is demonstrated not only with different target stoichiometries but also with improved morphologies and film compositions while changing the key deposition parameters: spot size and deposition pressure. The solvent-free nature of the current method during target production and the growth of films reduce the environmental impact of halide perovskite synthesis and increase the possibility of implementing this PVD method on a large scale. Future research venues include all-vacuum PVD-grown halide perovskites in a full solar cell structure. The lessons learned with the archetypical perovskite $MAPbI_3$ can also be applied to other hybrid compositions, including wide and low bandgap perovskites for monolithic tandem devices applications.

Acknowledgment

The authors acknowledge the European Research Council (ERC) financial support under the European Union's Horizon 2020 Research and Innovation Program (CREATE, Grant Agreement No. 852722) and the support of S.K by the Erasmus+ programme of the European Union. We acknowledge the CzechNanoLab Research Infrastructure supported by MEYS CR (LM2018110).

References

[1] H. S. Kim *et al.*, "Lead iodide perovskite sensitized all-solid-state submicron thin film mesoscopic solar cell with efficiency exceeding 9%," *Sci. Rep.*, vol. 2, pp. 1–7, 2012, doi: 10.1038/srep00591.

[2] J. S. Manser, J. A. Christians, and P. V. Kamat, "Intriguing Optoelectronic Properties of Metal Halide Perovskites," *Chem. Rev.*, vol. 116, no. 21, pp. 12956–13008, 2016, doi: 10.1021/acs.chemrev.6b00136.

[3] T. Soto-Montero, W. Soltanpoor, and M. Morales-Masis, "Pressing challenges of halide perovskite thin film growth," *APL Materials*, vol. 8, no. 11. 2020, doi: 10.1063/5.0027573.

[4] NREL, "Best Research-Cell Efficiencies," 2020.

[5] J. Kim *et al.*, "Overcoming the Challenges of Large-Area High-Efficiency Perovskite Solar Cells," *ACS Energy Lett.*, vol. 2, no. 9, pp. 1978–1984, 2017, doi: 10.1021/acsenergylett.7b00573.

[6] Y. Vaynzof, "The Future of Perovskite Photovoltaics—Thermal Evaporation or Solution Processing?," *Adv. Energy Mater.*, vol. 10, no. 48, 2020, doi: 10.1002/aenm.202003073.

[7] F. Sahli *et al.*, "Vapor Transport Deposition of Methylammonium Iodide for Perovskite Solar Cells," *ACS Appl. Energy Mater.*, 2021, doi: 10.1021/acsaem.0c02999.

[8] J. Ávila, C. Momblona, P. P. Boix, M. Sessolo, and H. J. Bolink, "Vapor-

Deposited Perovskites: The Route to High-Performance Solar Cell Production?," *Joule*, vol. 1, no. 3, pp. 431–442, 2017, doi: 10.1016/j.joule.2017.07.014.

[9] G. Koster, M. Huijben, and G. Rijnders, "Oxide superlattices by PLD: A practical guide," in *Metal Oxide-Based Thin Film Structures*, no. 001, Elsevier Inc., 2018, pp. 27–52.

[10] Y. Smirnov *et al.*, "Scalable Pulsed Laser Deposition of Transparent Rear Electrode for Perovskite Solar Cells," *Adv. Mater. Technol.*, vol. 6, no. 2, 2021, doi: 10.1002/admt.202000856.

[11] R. Eason, *Pulsed Laser Deposition of Thin Films*. Hoboken, New Jersey: John Wiley & Sons, Inc., 2007.

[12] A. Ojeda-G-P, M. Döbeli, and T. Lippert, "Influence of Plume Properties on Thin Film Composition in Pulsed Laser Deposition," *Adv. Mater. Interfaces*, vol. 5, no. 18, pp. 1–16, 2018, doi: 10.1002/admi.201701062.

[13] C. Momblona *et al.*, "Efficient vacuum deposited p-i-n and n-i-p perovskite solar cells employing doped charge transport layers," *Energy Environ. Sci.*, vol. 9, no. 11, pp. 3456–3463, 2016, doi: 10.1039/c6ee02100j.

[14] Y. H. Chiang, M. Anaya, and S. D. Stranks, "Multisource Vacuum Deposition of Methylammonium-Free Perovskite Solar Cells," *ACS Energy Lett.*, vol. 5, no. 8, pp. 2498–2504, 2020, doi: 10.1021/acsenergylett.0c00839.

[15] L. Gil-Escrig, C. Momblona, M. G. La-Placa, P. P. Boix, M. Sessolo, and H. J. Bolink, "Vacuum Deposited Triple-Cation Mixed-Halide Perovskite Solar Cells," *Adv. Energy Mater.*, vol. 8, no. 14, 2018, doi: 10.1002/aenm.201703506.

[16] V. M. Kiyek *et al.*, "Single-Source, Solvent-Free, Room Temperature Deposition of Black γ-CsSnI3 Films," *Adv. Mater. Interfaces*, 2020, doi: 10.1002/admi.202000162.

[17] N. Rodkey *et al.*, "Pulsed Laser Deposition of Cs2AgBiBr6: from mechanochemically synthesized powders to dry, single step deposition," *pending Rev.*

[18] U. Bansode, R. Naphade, O. Game, S. Agarkar, and S. Ogale, "Hybrid Perovskite Films by a New Variant of Pulsed Excimer Laser Deposition: A Room Temperature Dry Process Umesh," *J. Phys. Chem. C*, vol. 119, no. 17, pp. 1–5, 2015.

[19] H. Wang *et al.*, "Pulsed Laser Deposition of CsPbBr3 Films for Application in Perovskite Solar Cells," *ACS Appl. Energy Mater.*, vol. 2, no. 3, pp. 2305–2312, 2019, doi: 10.1021/acsaem.9b00130.

[20] U. Bansode and S. Ogale, "On-axis pulsed laser deposition of hybrid perovskite films for solar cell and broadband photo-sensor applications," *J. Appl. Phys.*, vol. 121, no. 13, 2017, doi: 10.1063/1.4979865.

[21] S. Hoffmann-Urlaub, Y. Zhang, Z. Wang, B. Kressdorf, and T. Meyer, "Fabrication of tin-based halide perovskites by pulsed laser deposition," *Appl. Phys. A Mater. Sci. Process.*, vol. 126, no. 7, pp. 1–11, 2020, doi: 10.1007/s00339-020-03699-9.

[22] N. Leupold and F. Panzer, "Recent Advances and Perspectives on Powder-Based Halide Perovskite Film Processing," *Adv. Funct. Mater.*, vol. 31, no. 14, 2021, doi: 10.1002/adfm.202007350.

[23] Z. Hong *et al.*, "Completely Solvent-free Protocols to Access Phase-Pure, Metastable Metal Halide Perovskites and Functional Photodetectors from the Precursor Salts," *iScience*, vol. 16, pp. 312–325, 2019, doi: 10.1016/j.isci.2019.05.042.

[24] D. Tan and F. García, "Main group mechanochemistry: from curiosity to established protocols," *Chem. Soc. Rev.*, vol. 48, no. 8, pp. 2274–2292, 2019, doi: 10.1039/c7cs00813a.

[25] M. Hu *et al.*, "Large and Dense Organic-Inorganic Hybrid Perovskite CH3NH3PbI3 Wafer Fabricated by One-Step Reactive Direct Wafer Production with High X-ray Sensitivity," *ACS Appl. Mater. Interfaces*, vol. 12, no. 14, pp. 16592–16600, 2020, doi: 10.1021/acsami.9b23158.

[26] N. Leupold *et al.*, "High Versatility and Stability of Mechanochemically Synthesized Halide Perovskite Powders for Optoelectronic Devices," *ACS Appl. Mater. Interfaces*, vol. 11, no. 33, pp. 30259–30268, 2019, doi: 10.1021/acsami.9b09160.

[27] S. De Wolf *et al.*, "Organometallic halide perovskites: Sharp optical absorption edge and its relation to photovoltaic performance," *J. Phys. Chem. Lett.*, vol. 5, no. 6, pp. 1035–1039, 2014, doi: 10.1021/jz500279b.

[28] L. Cojocaru *et al.*, "Detailed Investigation of Evaporated Perovskite Absorbers with High Crystal Quality on Different Substrates," *ACS Appl. Mater. Interfaces*, vol. 10, no. 31, pp. 26293–26302, 2018, doi: 10.1021/acsami.8b07999.

[29] J. B. Patel *et al.*, "Influence of Interface Morphology on Hysteresis in Vapor-Deposited Perovskite Solar Cells," *Adv. Electron. Mater.*, vol. 3, no. 2, pp. 1–6, 2017, doi: 10.1002/aelm.201600470.

[30] C. Altinkaya *et al.*, "Tin Oxide Electron-Selective Layers for Efficient , Stable , and Scalable Perovskite Solar Cells," *Adv. Mater.*, vol. 33, no. 15, p. 2005504, 2021, doi: 10.1002/adma.202005504.

[31] J. Li *et al.*, "Highly Efficient Thermally Co-evaporated Perovskite Solar Cells and Mini-modules," *Joule*, vol. 4, no. 5, pp. 1035–1053, 2020, doi: 10.1016/j.joule.2020.03.005.

[32] P. Lucke *et al.*, "Hysteresis, Loss and Nonlinearity in Epitaxial PbZr0.55Ti0.45O3 Films: A Polarization Rotation Model," *Adv. Funct. Mater.*, vol. 30, no. 52, pp. 1–12, 2020, doi: 10.1002/adfm.202005397.